Length scale parameters to estimate fatigue lifetime of 3D-printed titanium alloy Ti6Al4V containing notches in the as-manufactured condition

S.M.J. Razavi [a], H. Askes [b], F. Berto [a], L. Susmel [c],*

[a] Norwegian University of Science and Technology, NO-7491 Trondheim, Norway
[b] University of Twente, Faculty of Engineering Technology, Twente, Netherlands
[c] Department of Civil and Structural Engineering, The University of Sheffield, Mappin Street, Sheffield S1 3JD, United Kingdom

ARTICLE INFO

ABSTRACT

The accuracy of the Theory of Critical Distances, Gradient Elasticity and the Averaged Strain Energy Density criterion in estimating fatigue lifetime of notched additively manufactured Ti6Al4V is assessed against numerous experimental results generated under load ratios equal to −1 and 0.1. The 3D-printed Ti-alloy under investigation was tested by keeping the notches in the as-manufactured condition. The common feature of the considered design approaches is that they all make use of a material length scale. The validation exercise based on the generated experimental results demonstrates that the length scale concept can be extended successfully also to the fatigue assessment of notched 3D-printed metallic components.

1. Introduction

Additive Manufacturing (AM) is a group of fabrication processes that allow complex designs to directly be turned into physical components by an incremental addition of feedstock material supplied in the form of powder, wire and sheets. Compared to conventional fabrication processes, AM offers a wider range of advantages such as, for instance: elimination of expensive tools and moulds, lower material waste, higher flexibility in direct fabrication of complex CAD models, and, ultimately, faster time-to-market. Amongst the AM techniques for fabrication of metallic components available to date, certainly Laser Powder Bed Fusion (LPBF) is one of the most commonly used technologies in situations of practical interest. This process utilises a laser heat source to fuse the feedstock material supplied in the form of powder. Thanks to the ability of the LPBF process to make high quality parts containing intricate geometrical features, its application has been expanded so that it can be used to manufacture a wide range of different metallic materials - including Ti-alloys that are relevant for the present study.

The highly localised heat input during the LPBF process and the rapid cooling during the deposition of the layers result in a unique material microstructure. In particular, the microstructure is seen to be characterised by long grains elongated along the heat transfer direction, with this morphology potentially leading to an anisotropic mechanical behaviour [1]. Further, the use of this manufacturing process is seen to

result in brittle phases - such as, for instance, martensitic phases in steel and Ti-alloys - that can have a detrimental effect on the overall strength of the additively manufactured (AM) components. On top of that, the fabricated parts often have poor surface quality (mostly characterised by large residual stresses) and are likely to contain internal defects that manifest themselves in the form of trapped voids and lack of fusion between adjacent layers.

These process-driven characteristics directly influence the mechanical properties of LPBF-manufactured parts. Considering the local nature of fatigue failures, clearly these detrimental factors can act simultaneously and synergistically, with this resulting in further uncertainties in the material mechanical performance. These limitations explain the reason why much experimental/theoretical work has been done in recent years to improve the overall quality of LPBF-manufactured components, with this being achieved by: (i) optimizing the process parameters [2], (ii) formalising specific design procedures for additively manufactured components [3] and (iii) defining suitable post-processing treatments (e.g., heat and surface treatments) [4]. Accordingly, a well-optimized fabrication process can reduce the magnitude of the residual stresses, the level of the internal porosity, and the geometrical errors characterising the fabricated parts. In addition, process conditions such as preheating of both build stage and powder bed have shown to be effective in removing martensitic phases as well as in controlling the size of the grains during LPBF-manufacturing [4,5].

Turning to the design-related aspects, successful usage of AM

* Corresponding author.
E-mail address: l.susmel@sheffield.ac.uk (L. Susmel).

Nomenclature

2α	notch opening angle
B	body forces
cw	weighting parameter accounting for the load ratio
E_1	constant depending on the notch opening angle
k	negative inverse slope
ℓ	intrinsic material length scale determined according to GM
u	displacements
w_g	gross width
w_n	net width
A, B	constants in relationship $L(N_f)$
A_w, B_w	constants in the $\Delta\overline{W}$ vs N_f relationship
C_{ijkl}	matrix containing the elastic moduli
E	Young's modulus
F, H	geometrical functions used in the ASED criterion
K_t	stress concentration factor referred to the net area
L	high-cycle fatigue critical distance determined according to the TCD
$L(N_f)$	TCD critical distance in the finite life regime
L_{av}	average value of the TCD critical distance
N_f	number of cycles to failure
$N_{f,e}$	estimated number of cycles to failure
N_0	reference number of cycles to failure ($N_0 = 2\bullet10^6$ cycles to failure)
Oxyz	Cartesian coordinate system

Orθ	polar system of coordinates
P_S	probability of survival
R	load ratio ($R = \sigma_{min}/\sigma_{max}$)
R_0	critical radius determined according to the ASED criterion
T_σ	scatter ratio of endurance limit for 90 % and 10 % probabilities of survival
e_{ij}	Cartesian components of strains
$\lambda 1$	Mode I Williams' eigenvalue
σ_{ij}	Cartesian components of stresses
σ_{min}, σ_{max}	minimum/maximum stress in the cycle
ν	Poisson's ratio
r	notch root radius
ΔK_1	Mode I N-SIF range
$\Delta K_{1,A}$	Mode I N-SIF range of at the fatigue/endurance limit
ΔK_{th}	threshold value of the stress intensity factor range
$\Delta\overline{W}$	ASED range
$\Delta\sigma$	range of the nominal stress in the plain material
$\Delta\sigma_{eff}$	range of the TCD effective stress
$\Delta\sigma_1$	range of the maximum principal stress
$\Delta\sigma_{GE,y}$	range of the gradient-enriched stress at the notch tip
$\Delta\sigma_y$	range of the normal stresses parallel to the y-axis
$\Delta\sigma_{root}$	tensile stress range at the notch root
$\Delta\sigma_0$	range of the plain fatigue/endurance limit
$\Delta\sigma_{0n}$	range of the nominal net fatigue/endurance limit

involves effective selection of fabrication orientation, utilisation of supporting structures for better heat transfer during manufacturing and the incorporation of the process limits in the design procedures. As to the latter aspect, advanced topology optimization techniques can be used to fabricate AM components with minimal internal porosity, low magnitude of residual stresses and a more uniform surface finishing.

In terms of improving the overall mechanical performance, post-processing treatments have shown to be able to enhance significantly the mechanical properties of LPBF-manufactured metals to a level which is comparable with the conventional counterparts [6]. In this setting, heat-treatment of the as-fabricated LPBF parts is always recommended to improve the mechanical properties, with this being achieved by eliminating the residual stresses and by altering the material microstructure [7]. Hot Isostatic Pressing (HIP) is another well-known post-processing technology which is based on the simultaneous use of high pressure and high temperature to reduce the internal porosity [2,8]. However, since the HIP process does not mitigate the effect of the surface defects, it is recommended to be used along with other surface treatment techniques. In this context, sand blasting, shot peening and chemical etching have proven to be able to improve the surface quality of the AM parts, with this resulting in enhanced fatigue performance [9]. It is evident that synergistic usage of these post-AM techniques can result in the elimination of a number of detrimental AM-related factors, with this leading to enhanced mechanical performance.

Bearing in mind the advantages and limitations briefly summarised above, systematic effort has been made by the international scientific community to define standard procedures suitable not only for assessing the quality of AM components, but also for characterising their mechanical properties under various mechanical loading conditions. However, to the best of the authors' knowledge, there still is a lack of specific standardised procedures to be followed to assess structural integrity, with the majority of the available research studies attempting to use with 3D-printed parts specific methodologies originally developed for conventionally manufactured metallic components [10].

As far as metal fatigue is concerned, the localised nature of this type of failures implies that in structural components cracks usually initiate in small material volumes in the vicinity of geometrical discontinuities acting as stress/strain concentrators. Owing to such a localised nature, it is common practice to use local approaches to perform fatigue assessment of real components. The common feature characterising these design methods is that fatigue failures are assumed to take place when the magnitude of a key parameter - such as stress, strain, strain energy density (SED), etc. - determined by post-processing the stress/strain fields in the vicinity of the crack initiation locations reaches a material-dependant critical value [11]. In general terms, the key design parameter is either extracted at a single point (Point Method), averaged over a line (Line Method), or averaged in a control bi-dimensional/three-dimensional domain (Area/Volume Method).

In this challenging scenario, the ultimate goal of the present investigation is to check the accuracy and reliability of the Theory of Critical Distances (TCD), Gradient Elasticity (GE), and the Averaged Strain Energy Density (ASED) in estimating fatigue lifetime of LPBF-manufactured notched specimens of Ti-6Al-4 V when this AM Ti-alloy is employed with the notch region being kept in the as-manufactured condition. While these three design approaches are different in their details, they share two common fundamental features:

- fatigue damage is estimated via a length scale parameter that is linked with the micro/*meso*-structure of the material under investigation;
- the stress/strain analysis is performed based on a simple linear-elastic constitutive law.

Considering the distinctive characteristics of AM metallic materials, the accuracy of the TCD, GE, and the ASED method in estimating uniaxial fatigue lifetime of notched LPBF-AM Ti-6Al-4 V is assessed against a large number of experimental results generated in our laboratories. To this end, the fundamentals of these three methods are reviewed in the following three sections. Subsequently, the experimental results generated by testing plain and notched specimens of LPBF-AM Ti-6Al-4 V are presented, summarised and discussed. In the last part of the work, the accuracy of the three critical length-based approaches being considered

is assessed quantitatively against the produced fatigue data, with the key conclusions being drawn in the last section.

2. Basics of the Theory of Critical Distances

As far as fatigue assessment is concerned, the TCD [12–16] estimates the extent of damage via a material length scale parameter which is used to post-process the local linear-elastic stress fields in the vicinity of the assumed crack initiation locations. In the TCD framework, the critical distance is treated as a material property, with this length varying as the load ratio, R, increases [14,16]. Based on the above idea, the different formulations of the TCD can be derived by simply changing the characteristics of the integration domain used to quantify the design effective stress, $\Delta\sigma_{eff}$ [13,17].

The three-dimensional formalisation of the TCD (which is known as the Volume Method) calculates $\Delta\sigma_{eff}$ by averaging the time-variable local-linear elastic stresses in a hemisphere which is centred at the tip of the assessed notch/crack [17]. Accordingly, the TCD used in the form of the Volume Method estimates fatigue damage in the presence of stress concentrators by directly manipulating the local linear-elastic stress field acting on a specific material process zone [18]. In this setting, this process zone can be treated as that portion of material which controls the overall fatigue strength of the component being designed. From a materials science viewpoint, the size of the process zone (and, therefore, the length of the TCD critical distance) depends on the characteristics/features of the local material microstructural heterogeneities, on the mechanical/cracking behaviour at micro-*meso*-scopic level as well as on the size of the plastic region [16,18].

As far as the fatigue/endurance limit problem is concerned, the TCD critical distance can be calculated according to the following well-known relationship [12,13,19]:

$$L = \frac{1}{\pi}\left(\frac{\Delta K_{th}}{\Delta\sigma_0}\right)^2 \tag{1}$$

where ΔK_{th} is the range of the threshold value of the stress intensity factor, whereas $\Delta\sigma_0$ is the plain fatigue/endurance limit.

Since, as said above, the TCD critical distance depends also on the size of the plastic region, it is seen to increase as the magnitude of the applied cyclic loading increasing [20,21]. From a fatigue strength point of view, this implies that the TCD critical distance increases as the number of cycles to failure, N_f, decreases. Accordingly, the relationship between critical distance and N_f can be expressed directly via a simple power law [20]:

$$L(N_f) = A \bullet N_f^B \tag{2}$$

In Eq. (2) A and B are material fatigue constants that can be determined by running appropriate experiments. For a given material, constants A and B vary as the load ratio changes. In contrast, the values of A and B do not vary as profile and sharpness of the assessed stress concentrator change. The procedure being recommended to calibrate function (2) will be discussed in detail at the end of the present section.

The evident conceptual/physical links between its *modus operandi* and the three-dimensional process zone concept make the Volume Method very appealing from a scientific point of view. However, unfortunately, its usage in situations of practical interest is not at all straightforward because $\Delta\sigma_{eff}$ can be calculated provided that the local stress fields are determined and integrated accurately in the control volume. Clearly, this can be a very laborious task since suitable numerical/analytical tools are required in the presence of complex, three-dimensional components so that the local linear-elastic stresses are averaged accurately over the relevant integration domains. The above obstacle can be overcome by using the other formalisations of the TCD which are, by their nature, simpler to apply. These different forms of the TCD are briefly reviewed in what follows.

According to the Area Method (which is the bi-dimensional version

of the TCD) $\Delta\sigma_{eff}$ can be determined by directly averaging the local linear-elastic stresses over a semi-circular area centred at the tip of the assessed stress concentrator and having radius equal to $L(N_f)$ [13,22]. From a mathematical point of view, the effective stress can be determined according to the Area Method as follows [13] (see also Fig. 1a and d):

$$\Delta\sigma_{eff} = \frac{4}{\pi L(N_f)^2}\int_0^{\pi/2}\int_0^{L(N_f)}\Delta\sigma_1(\theta,r).r.dr.d\theta \tag{3}$$

where $\Delta\sigma_1$ is the range of maximum principal stress.

The one-dimensional formalisation of the TCD is known as the Line Method. It postulates that $\Delta\sigma_{eff}$ has to be determined by averaging the local linear-elastic stress along a linear path having length equal to 2L, i.e. [13] (see also Fig. 1a and 1c):

$$\Delta\sigma_{eff} = \frac{1}{2(N_f)}\int_0^{2L(N_f)}\Delta\sigma_y(\theta=0,r)\bullet dr \tag{4}$$

where, as per Fig. 1c, $\Delta\sigma_y$ is the normal stress parallel to the y-axis.

Lastly, the zero-dimensional form of the TCD is called the Point Method and assumes that $\Delta\sigma_{eff}$ is equal to the linear-elastic stress determined at a distance of L/2 from the notch/crack apex, i.e. [12,13] (see also Fig. 1a and 1b):

$$\Delta\sigma_{eff} = \Delta\sigma_y\left(\theta=0,r=\frac{L(N_f)}{2}\right) \tag{5}$$

Independently of the strategy being used to determine Δ_{eff}, the last step in the design process is to estimate fatigue lifetime from the plain material fatigue curve (experimentally determined under the appropriate load ratio) as follows [20]:

$$N_{f,e} = N_0\left(\frac{\Delta\sigma_0}{\Delta\sigma_{eff}}\right)^k \tag{6}$$

In Eq. (6) $N_{f,e}$ is the estimated number of cycles to failure, $\Delta\sigma_0$ is the un-notched material endurance limit range extrapolated at N_0 cycles to failure and k is the negative inverse slope of the plain fatigue curve.

By focusing attention on definition (2), it is straightforward to observe that $N_{f,e}$ is needed to determine the critical distance value used to calculate the effective stress according to Eqs (3) to (5). However, in a fatigue design context, obviously the number of cycles to failure represents the unknown variable in the problem. Therefore, as discussed in detail in Ref. [20], the TCD can be employed to predict fatigue lifetime of notched components provided that suitable recursive numerical procedures are employed.

The last aspect to be considered in the present section is the determination of material constants A and B in Eq. (2). As recommended in Ref. [20], this can be done by post-processing the un-notched material fatigue curve together with another fatigue curve determined by testing specimens weakened by a known geometrical feature. This simple and straightforward approach to calibrate relationship $L(N_f)$ is explained in Fig. 1e. In more detail, for given a number of cycles to failure, N_f^*, it is possible to estimate the distance from the notch/crack tip, $L(N_f)/2$, at which the linear-elastic stress range, $\Delta\sigma_y$, equals the range of the stress, $\Delta\sigma^*$, that has to be applied to break the un-notched material at N_f^* cycles to failure (Fig. 1e). Via this simple procedure based on the Point Method, the TCD critical distance can then be determined at different numbers of cycles to failure, with this resulting in an unambiguous determination of constants A and B in Eq. (2). This straightforward calibration strategy will be employed below to assess the accuracy of the linear-elastic TCD in estimating fatigue lifetime of notched AM Ti6Al4V.

3. Basics of Gradient Elasticity

An alternative (though, as we will demonstrate, quantifiably comparable) approach to assess the stress fields around stress raisers is
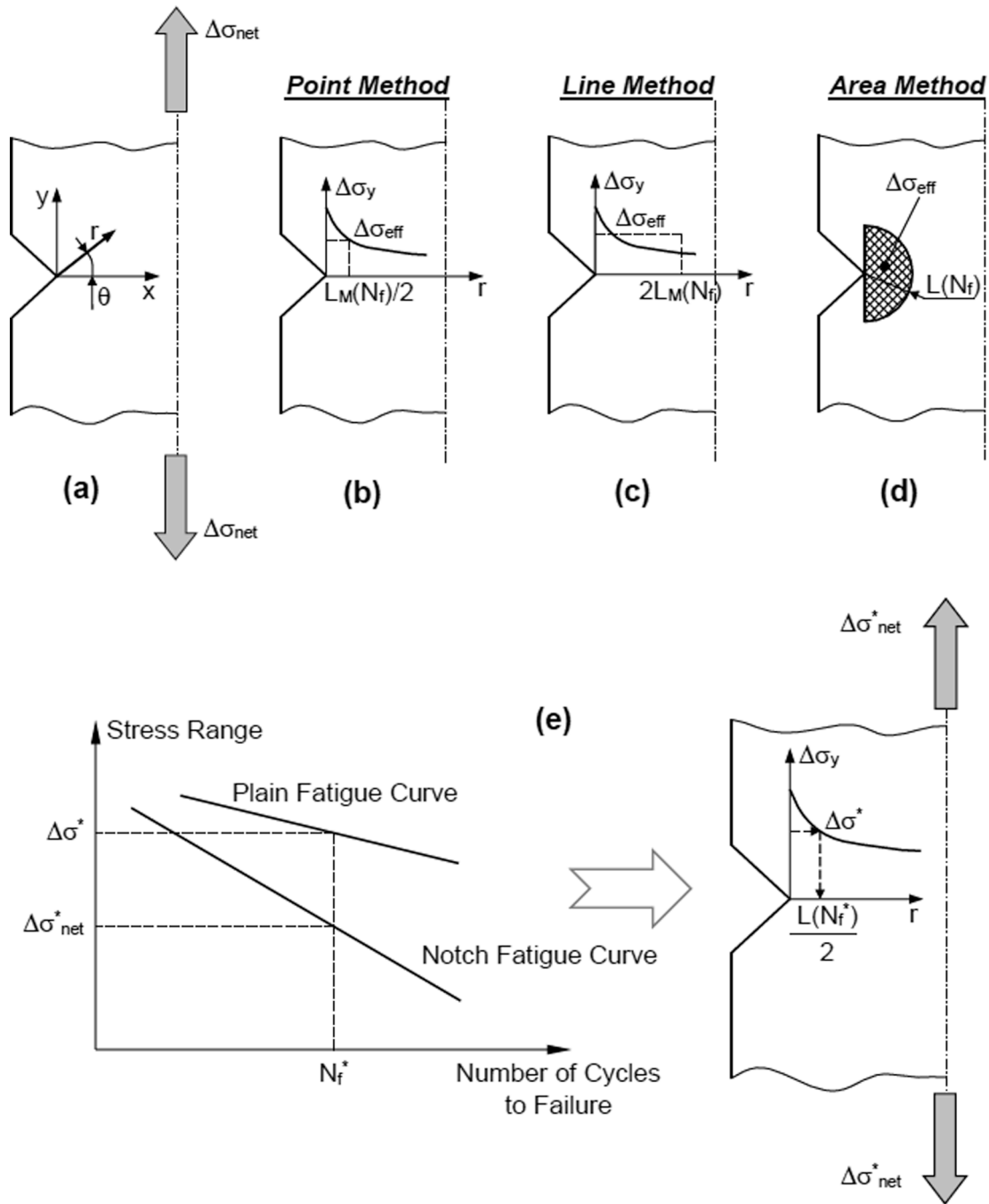
Fig. 1. Notched component subjected to fatigue loading (a); effective stress calculated according to the Point (b), Line (c) and Area Method (d); calibration of the L (N$_f$) relationship via a plain fatigue curve and a notch fatigue curve (e).

provided by generalized continuum theories, in particular the theory of GE as advocated by Aifantis and co-workers [23–25].

The analogies and similarities between the TCD and GE can be understood via the concept of nonlocal elasticity [26,27], whereby weighted volume averages of stress quantities are computed using certain weighting functions. Taking these weighting functions as unity inside a hemisphere and zero outside leads to the Volume Method of the TCD; similarly, unit weighting functions in a semi-circle or along a line segment leads to the Area Method and the Line Method of the TCD, whereas taking a Dirac delta function as a weighting function results in the Point Method. On the other hand, Eringen showed that a higher-order *differential relation* between stresses and strains is obtained when the nonlocal weighting function is taken as a Green's function [28].

Thus, nonlocal mechanics provides the framework that unifies the TCD and generalized continuum mechanics.

In the 1990 s, Aifantis and co-workers suggested to extend the stress–strain relations with the Laplacian of the strain [23–25], as follows:

$$\sigma_{ij} = C_{ijkl}\left(\varepsilon_{kl} - \ell^2 \varepsilon_{kl,mm}\right) \tag{7}$$

where σ_{ij} and ε_{ij} are the Cartesian components of stresses and strains, C_{ijkl} contains the elastic moduli, and indices following a comma denote derivation with respect to the relevant spatial coordinate. The Laplacian of the strain is accompanied by an additional material parameter ℓ that has the unit of length and is envisaged to capture the geometry of the material's microstructure; this new material parameter is often called

the *internal* or *microstructural* length scale.

The equilibrium equations based on Eq. (7) in terms of displacements u_i read:

$$C_{ijkl}\left(u_{k,jl} - \ell^2 u_{k,jlmm}\right) + b_i = 0 \tag{8}$$

where the body forces are denoted as b_i.

To facilitate analytical and numerical solution methods, Ru and Aifantis [25] suggested to factorise the various derivatives in Eq. (8) as:

$$C_{ijkl}\left(u_k - \ell^2 u_{k,mm}\right)_{jl} + b_i = 0 \tag{9}$$

This allows to interpret the quantity inside the parentheses as the displacements of the classical theory of elasticity, and indicates that the fourth-order differential equation (9) can be solved as a sequence of two second-order differential equations:

$$C_{ijkl}u^c_{k,jl} + b_i = 0 \tag{10a}$$

$$u^g_k - \ell^2 u^g_{k,mm} = u^c_k \tag{10b}$$

where superscripts *c* and *g* denote the classical and gradient-enriched fields, respectively. It is easily verified that substituting Eq. (10b) back into Eq. (10a) leads to Eq. (9); however, the variationally consistent boundary conditions that accompany Eqs (10) differ from those of Eq. (9). To reduce this effect, it was suggested [29] to take the derivative of Eq. (10b) and pre-multiply it with the constitutive tensor C_{ijkl} to arrive at a stress-based counterpart of Eq. (10b):

$$\sigma^g_{ij} - \ell^2 \sigma^g_{ij,mm} = C_{ijkl}u^c_{k,l} \tag{10c}$$

The response of this stress-based staggered formulation of GE according to Eqs. (10a) and (10c) was shown to be the closest to that of the original formulation of Eq. (8), although some quantitative differences remain due to the format of the variationally consistent boundary conditions. An additional advantage of Eqs. (10a) and (10c) is that they contain second-order differential equations; thus, numerical implementation with the finite element method is straightforward [29,30].

However, of particular interest to the present paper is the strong similarity between this stress-based staggered gradient elasticity approach and the TCD: both of these are based on first solving the equations of classical elasticity, and subsequently post-processing these via one or other approach of nonlocality. The unifying concept of non-locality can also be used to derive a relation between the internal length scale ℓ of gradient elasticity and the critical distance *L* of the TCD. Using a truncated Taylor series expansion in the Area Method of the TCD, it was shown [31] that the two length parameters are related via.

$$\ell^2 \approx \tfrac{1}{8}L^2 \text{ or } \ell\left(N_f\right) \approx \tfrac{1}{8}L\left(N_f\right)^2 \tag{11}$$

With this relation, it has been shown that gradient elasticity is able to capture a wide range of experimental results related to the fracture strength as well as fatigue limit of engineering structures and components [31–34].

4. Basics of the averaged strain Energy density approach

The volumetric formulation of the Strain Energy Density (SED) proposed by Lazzarin and Zambardi [35] assumes that engineering materials fail when the SED averaged in a control volume in the vicinity of the crack/notch under investigation reaches a critical value. This critical value is postulated to be independent of the notch geometry so that it depends solely on the mechanical properties of the material being designed. This criterion, known as the Average Strain Energy Density (ASED) approach, has been applied successfully to assess a large variety of brittle, quasi-brittle and ductile materials and its robustness and reliability in predicting failure of cracked and notched components under quasi-static loading are well documented (see Ref. [36] and references reported therein). Owing to such a remarkable level of accuracy, the idea the original formulation of the ASED approach is based on was

then extended to fatigue situations, with this being done by initially post-processing a large number of fatigue data generated by testing welded joints. In this setting, the pivotal idea was to use the ASED calculated in a control volume of a certain size instead of the stress in the net section of the welded components. The resulting unifying fatigue curve was found to be independent of the weld geometry. Accordingly, it was treated as a master curve which can be used for fatigue life prediction of welded components without the need for performing new fatigue experiments.

Calculation of the local SED around geometrical discontinuities requires precise information on the size of the control volume in which the SED itself is averaged. Theoretically, the material properties around the notch tip depend on a number of factors including (but not limited to) microstructure, surface roughness, internal defects, and residual stresses. Accordingly, developing an ASED-based approach which can be used to predict fatigue life of AM components is obviously a challenging task. To this end, the ASED criterion makes use of a simplified methodology to estimate fatigue lifetime of AM notched components, where the size of the control volume is determined by treating the effect of the various influencing factors in statistical terms [1]. In particular, based on the ASED criterion, the size of the control volume around the notch tip is estimated by using the fatigue strength characterising two reference geometries, i.e., plain material and V-notch. By so doing, in the absence of any global stress/strain raiser, the effect of surface roughness and internal defects is modelled via the fatigue results generated by testing plain specimens [35]. A schematic illustration of the control volume for sharp and blunt notch geometries is given in Fig. 2 [37]. In this figure, 2α is the notch opening angle, ρ is the notch root radius, R_0 is the critical radius defining the size of control volume, and r_0 is the distance between the centre of the control volume and the notch tip in a blunt notch, with r_0 being defined as: $r_0 = \rho \bullet (\pi - 2\alpha)/(2\pi - 2\alpha)$. For cracks and sharp notches, the control volume is defined as a circle having radius equal to R_0 and centred at the crack/notch tip. The critical radius in plane-strain condition can be calculated using the following expression [35]:

$$R_0 = \left(\frac{\sqrt{2e_1}\,\Delta K_{1A}}{\Delta\sigma_0}\right)^{\frac{1}{1-\lambda_1}} \tag{12}$$

where constant e_1 depends on the notch opening angle, 2α, ΔK_{1A} is the mode I Notch-Stress Intensity Factor (*N*-SIF) range of the reference notched specimen at the fatigue/endurance limit, $\Delta\sigma_0$ is the fatigue/endurance limit of the plain material and λ_1 is Williams' eigenvalue [38]. The Mode I *N*-SIF in this equation can be calculated according to the following expression (see Fig. 1a for the adopted system of coordinates):

$$\Delta K_1 = \sqrt{2\pi} \lim_{r \to 0^+} r^{1-\lambda_1} \Delta\sigma_y(r, \theta = 0) \tag{13}$$

For a given stress range $\Delta\sigma$, the ASED range for plain specimens is defined as:

$$\Delta\overline{W} = \frac{c_w(\Delta\sigma)^2}{2E} \tag{14}$$
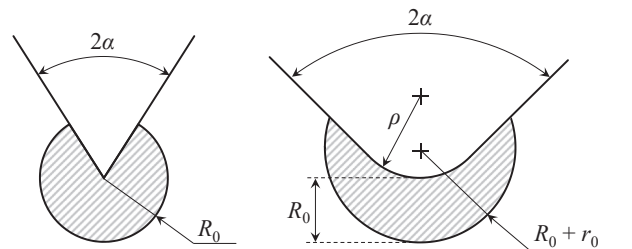

Fig. 2. ASED control volume around sharp and blunt V-notch under mode I loading condition [37].

where E is Young's modulus. Weighting parameter c_w is used in this expression to account for the effect of the nominal load ratio, $R = \sigma_{min}/\sigma_{max}$. This weighting parameter can be calculated using the following expression [39,40]:

$$c_w = \begin{cases} \dfrac{1 + R^2}{(1 - R^2)} for -\infty \leq R < 0 \\ 1 for R = 0 \\ \dfrac{1 + R^2}{(1 - R^2)} for 0 \leq R < 1 \end{cases} \quad (15)$$

For sharp notches, the SED averaged in the control volume can directly be computed using the following equation as a function of the *N*-SIF range, the elastic modulus, and the critical radius [41]:

$$\Delta\overline{W} = c_w \frac{e_1}{E} \left(\frac{\Delta K_1^2}{R_0^{2(1-\lambda_1)}} \right) \quad (16)$$

Dealing with blunt notches under Mode I loading, the ASED range can be expressed as a function of the tensile stress range at the notch root according to the following closed-form equation [42]:

$$\Delta\overline{W} = c_w \bullet F(2\alpha) \bullet H\left(2\alpha, \frac{R_0}{\rho}\right) \bullet \frac{\Delta\sigma_{root}^2}{E} \quad (17)$$

where F is a geometrical function that depends on notch opening angle 2α, H is a function that depends on both notch opening angle 2α and the ratio between critical radius and notch root radius (i.e., R_0/ρ) and $\Delta\sigma_{root}$ is the tensile stress range at the notch root.

Finite Element (FE) analysis can be employed to calculate the ASED as an alternative strategy to the use of the theoretical formulas briefly reviewed above. By so doing, the ASED values for notched components can directly be extracted by post-processing simple linear-elastic FE models. Since the SED values can be determined using the nodal displacements without involving their derivatives, their calculation do not require the use of a very fine mesh in the regions of interest [43]. This means that the local ASED is independent of the mesh size and it can be determined with high level of accuracy by simply using regular coarse meshes.

To summarize, the ASED approach is applied by estimating the size of the control volume via Eq. (12) from experimental results generated by investigating two reference geometrical configurations (i.e. plain and sharply notched specimens). Alternative procedures for the calculation of the critical radius in the ASED approach can be found in Ref. [1]. As soon as the critical size of the control volume is known, the ASED ranges for plain and notched specimens generated experimentally can be used to plot the corresponding $\Delta\overline{W}$ vs N_f diagram. These data form the basis of the master curve and are used to obtain the constants in a regression equation that can be written as: $\Delta\overline{W} = A_w \bullet N_f^{B_w}$. This equation can then be employed to predict the fatigue lifetime, N_f, of other components containing different geometrical features, with this holding true provided that they are fabricated using the same material and the same manufacturing procedures. The predictions obtained using this method shed light on the minimum allowable fillet radius to be used in geometrically complex AM parts.

The ASED criterion has been widely used over the last two decades with a wide range of materials and loading conditions. Numerous advantages have been reported for this criterion such as the simplicity of the method, its ability to consider the effect of loading ratio, *T*-stress, mode mixity, and, ultimately, its accuracy in modelling the scale and three-dimensional effect.

5. Experimental details

To assess the accuracy of the methodologies reviewed in the previous sections in estimating fatigue lifetime of 3D-printed metals containing notches in the as-manufactured condition, plain and notched specimens of AM Ti6Al4V were tested under cyclic axial loading in the laboratories of the University of Sheffield, UK.

The specimens being used were fabricated at the Norwegian University of Science and Technology, Trondheim, via the Direct Metal Laser Sintering (DMLS) technology. In particular, 3D-printer EOS M280 (with maximum laser power of 400 W) was employed by setting the laser power equal to 280 W, the scan speed to 1200 mm/*sec* and the hatch distance to 0.140 mm. Both the plain and the notched samples were manufactured flat on the build plate. The specimens were deburred and lightly polished in order to markedly reduce the surface roughness. All the samples were tested by keeping the notches in the as-manufactured condition. In particular, no post-fabrication high-temperature/high-pressure curing was employed to mitigate, in the notch regions, the detrimental effect of manufacturing defects and superficial residual stresses.

The titanium alloy additively manufactured according to the procedure briefly discussed above had Young's modulus, E, equal to 110 GPa, ultimate tensile strength, σ_{UTS}, equal to 1413 MPa and Poisson's ratio, ν, to 0.33.

According to the pictures seen in Fig. 3, both the plain and the notched specimens had average thickness equal to 2.7 mm and average gross width, w_g, equal to 12.1 mm. The average width, w_n, of the gauge section in the un-notched specimens was equal to 4.6 mm. The sharply V-notched specimens had average net width, w_n, equal to 4.7 mm, average notch root radius, ρ, equal to 0.4 mm and average notch opening angle equal to 35°. The intermediate U-notched specimens had average net width equal to 5.8 mm and average notch root radius equal to 0.7 mm. The bluntly U-notched samples had w_n equal to 6.0 mm and ρ to 1.5 mm.

The fatigue tests were run at a frequency of 10 Hz by employing a walter + bai 25 kN servo-hydraulic fatigue testing machine (Model LFV-25-ME) controlled through digital controller walter + bai PCS8000. All the tests were run at room temperature under sinusoidal constant-amplitude axial loading. The fatigue results were generated under nominal load ratios, R, equal to −1 as well as to 0.1.

Owing to the fact that the net cross-sections of the samples being tested were very small, fatigue failures were defined as the number of cycles resulting in the complete separation of the specimens. The post-processing of the force/displacement signals directly gathered from the fatigue machine showed that final breakages were never preceded by any gradual decrease in the stiffness. This confirms that, given the reduced dimensions of the cross-sectional areas and the characteristics of the material being tested, the propagation of the fatigue cracks occurred almost instantaneously under the maximum force applied in the cycle. This also means that the propagation process did not result in any secondary bending effects. Further the direct inspection of the fracture surfaces revealed that, due to the almost instantaneous nature of the process, the crack propagation phase was not affected by the superficial scratches in the notch region. In contrast, the profile of the crack propagation paths was seen to depend on the actual local morphology of the material at the net section of the individual specimens. The run-out tests were all stopped at $2\bullet10^6$ cycles. The matrix of failures reported in Fig. 4 shows some representative examples of the crack initiation paths that were observed both in the plain and in the notched specimens under load ratios equal to −1 as well as to 0.1.

The raw data generated by following the above experimental protocol are summarised in the SN log–log diagrams of Fig. 5. The stress amplitudes, $\sigma_{net,a}$, used to build the charts displaying the notch fatigue results were calculated by referring to the net nominal area. The scatter bands plotted in the diagrams of Fig. 5 were determined by assuming a log-normal distribution of the number of cycles to failure for each stress level with a confidence level equal to 95 %, [44,45]. The results from the statistical re-analyses are summarised also in Table 1 in terms of negative inverse slope, k, endurance limit range, $\Delta\sigma_0$ or $\Delta\sigma_{0n}$, extrapolated, for a probability of survival, P_S, equal to 50 %, at $N_0 = 2\bullet10^6$ cycles to

Plain Specimen – K$_t$=1

Blunt notch – K$_t$=2.10

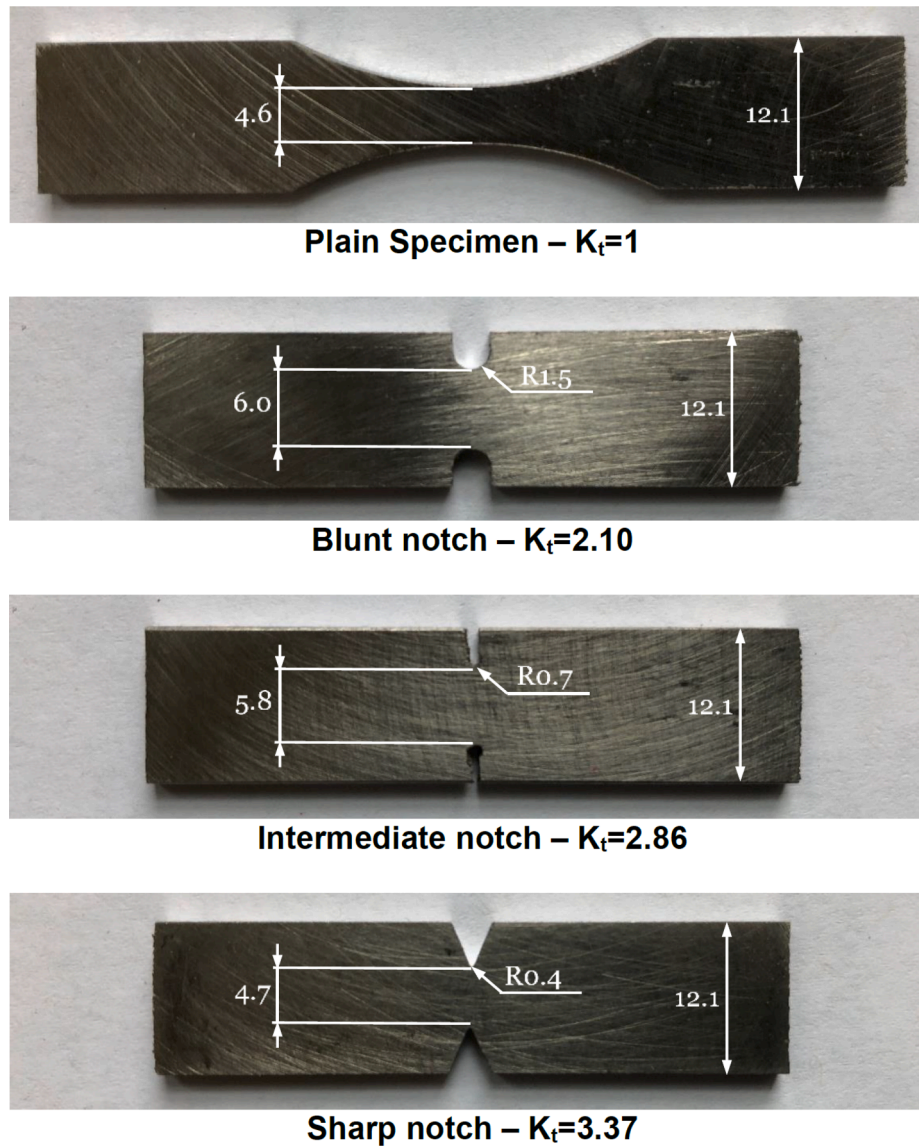**Intermediate notch – K$_t$=2.86**

Sharp notch – K$_t$=3.37

Fig. 3. Geometry of the tested specimens and average dimensions (average thickness equal to 2.7 mm).

failure, and, finally, scatter ratio, T$_\sigma$, of the endurance limit for 90 % and 10 % probabilities of survival. In Table 1 $\Delta\sigma_0$ is used to denote the plain material endurance limit range, whereas $\Delta\sigma_{0n}$ is the nominal notch endurance limit range referred to the net area. Accordingly, scatter ratio T$_\sigma$ is defined as follows:

$$T_\sigma = \frac{\Delta\sigma_{0,P_S=10\%}}{\Delta\sigma_{0,P_S=90\%}} \text{ for plain curves} \tag{18}$$

$$T_\sigma = \frac{\Delta\sigma_{0n,P_S=10\%}}{\Delta\sigma_{0n,P_S=90\%}} \text{ for notch curves} \tag{19}$$

The charts of Fig. 5 together with the results summarised in Table 1 make it evident that the presence of manufacturing defects resulted in relatively large values of scatter ratio T$_\sigma$. It is interesting to observe that, for a given notch geometry, the level of scattering was not affected by the load ratio, R, being applied. In this setting, the exception is represented by the data generated by testing the intermediate notches (i.e., notches with ρ = 0.7 mm), where the presence of relatively big manufacturing defects in some of the samples resulted in a T$_\sigma$ value of 7.32 under R = -1. It has to be said that a T$_\sigma$ value of 7.32 is certainly very high. However, these data were in any case included in the re-analyses discussed below for the following reason. Additively

manufactured components always contain defects and/or voids that are randomly introduced during the fabrication process. Since they act as local stress concentrators, these manufacturing flaws have a detrimental effect on the overall fatigue strength of 3D-printed components. The ultimate goal of the present research work is to assess the accuracy of three different length scale-based design tools in performing the fatigue assessment of 3D-printed metals containing notches in the as-manufacture condition. Owing to the fact that fabrication defects are a relevant aspect of the additive manufacturing technology, it is certainly relevant to assess the accuracy of the design criteria being investigated also when the fatigue behaviour of the considered experimental results is markedly affected by the presence of flaws. This explains the reason why the data generated under R = -1 by testing notch specimens with ρ = 0.7 mm were considered in the validation exercise discussed in the next section even though the corresponding scatter band was characterised by a T$_\sigma$ value of 7.32.

Another important aspect to be considered in detail is that the plain fatigue curves were seen to be characterised by a very low value of the negative inverse slope – i.e. k = 2.8 under R = -1 and k = 3.3 under R = 0.1 (Tab. 1). These k values are way lower than those usually displayed by un-notched metallic materials, with conventional metals having a negative inverse slope under uniaxial loading in the range 8–12 (if not
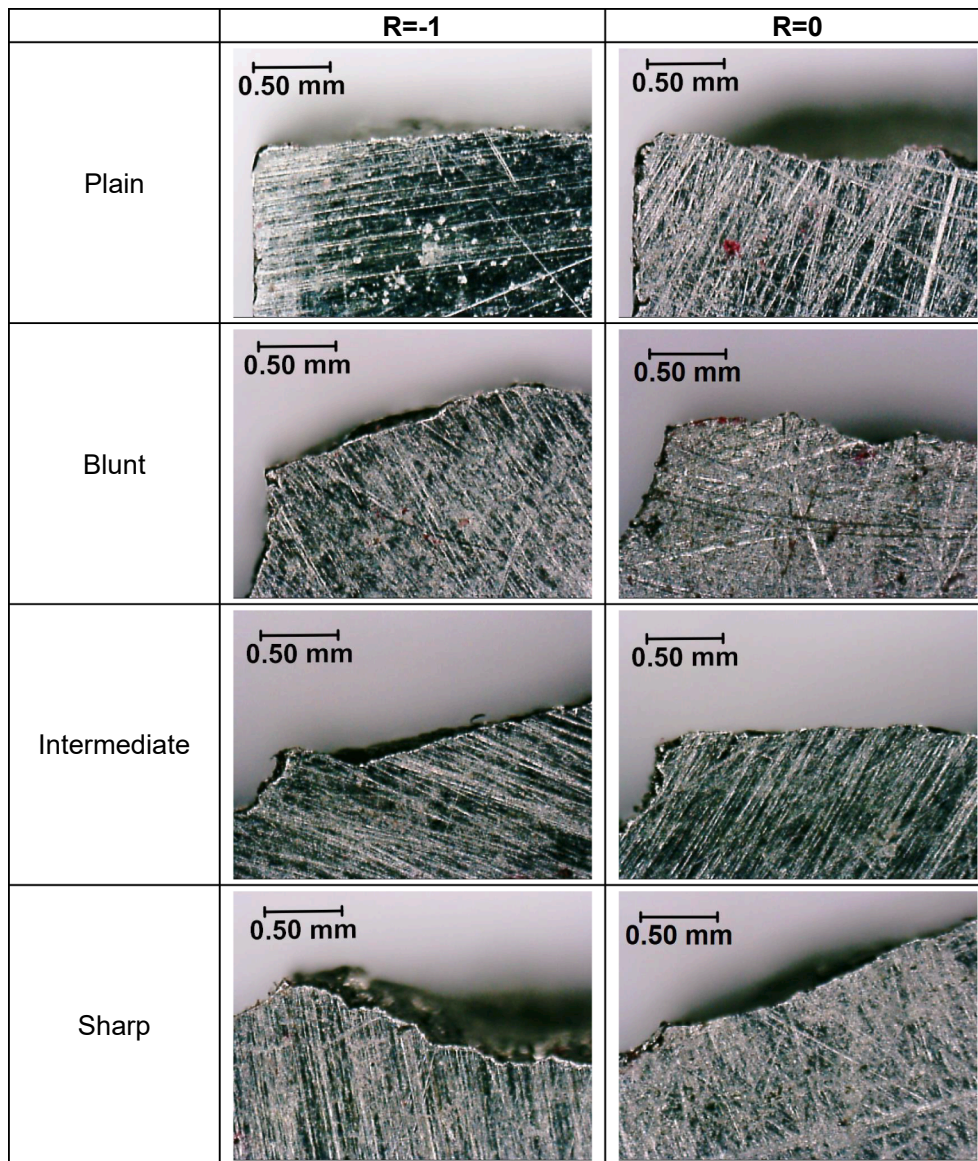
Fig. 4. Examples of the macroscopic cracking behaviour displayed by the tested plain and notched specimens of AM Ti6Al4V (in the pictures the specimen's longitudinal axes are vertical and the crack initiation points/notch tips are on the left-hand side).

larger) [46]. These low values for k can be ascribed to the detrimental effect of the manufacturing defects whose presence resulted, from a fatigue point of view, in an intrinsically notched material. In contrast, in the specimens containing geometrical features the stress concentration phenomena associated with the manufacturing flaws were somehow hidden by the presence of the conventional macroscopic notches. As a result, the plain fatigue curves were seen to be characterised by k values close to the negative inverse slope values displayed by the notch fatigue curves (see Fig. 5 and Table 1).

As far as the effect of the manufacturing defects is concerned, it can be pointed out also that, compared to the experimentally determined ultimate tensile strength, the fully-reversed plain material endurance limit was seen to be very low. In particular, it is well-known that in conventional metallic materials, the ratio between $\Delta\sigma_0/2$ (under R = -1) and σ_{UTS} is equal to approximately 0.5 [46,47]. In contrast, this ratio for the titanium alloy being investigated was experimentally determined to be equal to 0.07. This suggests that, while the internal flaws introduced during the additive manufacturing process just marginally influenced the material static strength, their presence had instead an evident detrimental effect on the overall fatigue performance of the AM titanium

alloy being investigated.

6. Validation

The local-stress distributions in the vicinity of the investigated stress concentrators were determined according to classic continuum mechanics by using commercial Finite Element (FE) code ANSYS®. The notched specimens seen in Fig. 3 were modelled as bi-dimensional bodies by using 4-node structural plane elements (plane 182). As recommended in Ref. [20], the relevant stress fields were determined by treating the AM titanium alloy under investigation as a linear-elastic, homogeneous and isotropic material. In order to determine the required local linear-elastic stress fields with the necessary level of accuracy, the mesh density in the notch regions was gradually increased until convergence occurred.

Based on these standard numerical solutions, the net stress concentration factor, K_t, was calculated to be equal to 2.10, 2.86 and to 3.37 for the specimens containing blunt, intermediate and sharp notches, respectively (see also Fig. 3 and Table 1).

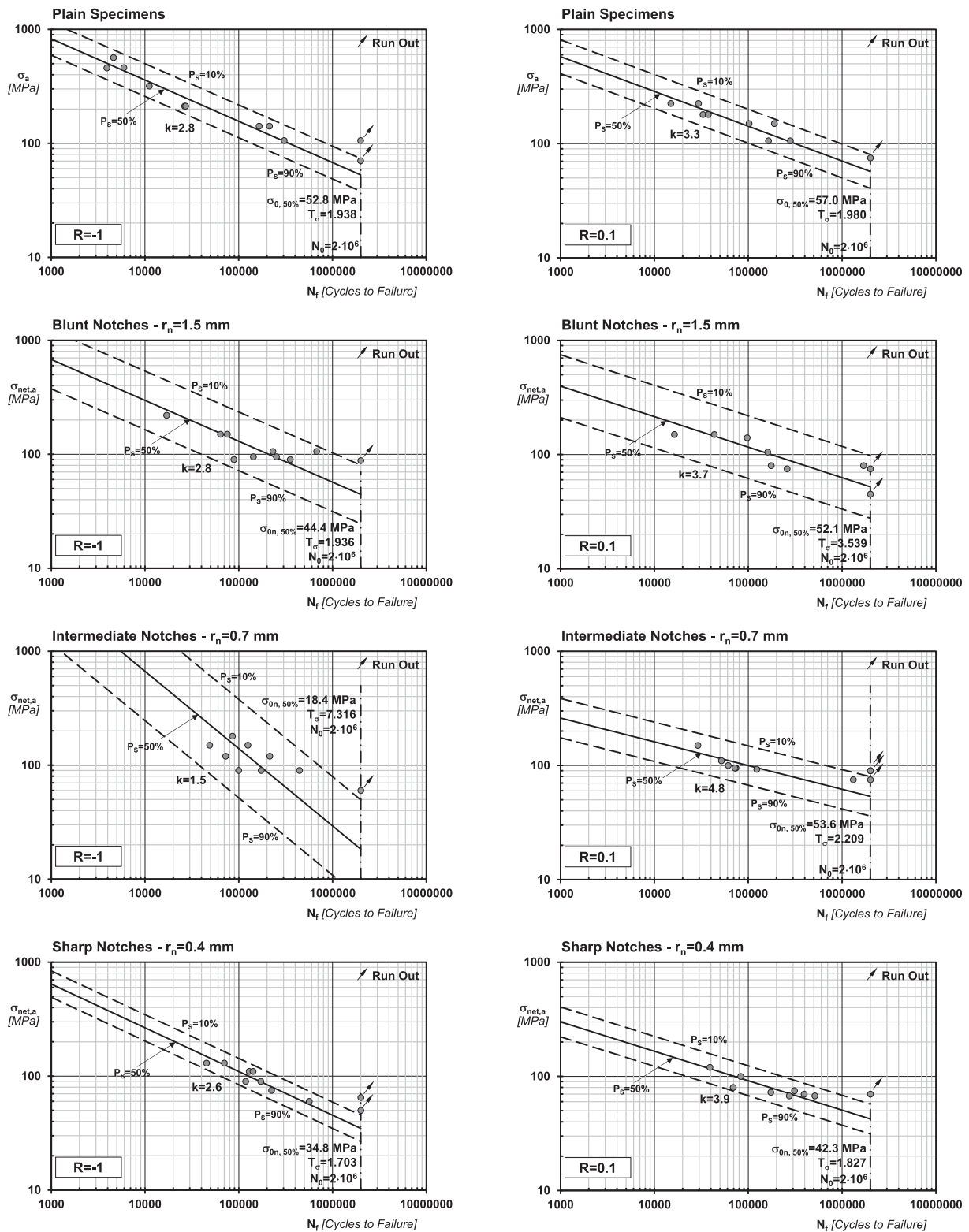The solutions from the standard FE analyses briefly described above

Fig. 5. Fatigue curves and associated scatter bands determined by post-processing the experimental data generated by testing plain and notched specimens of AM Ti6Al4V.

were initially used to check the accuracy of the TCD in estimating the notch results summarised in Fig. 5.

As per the calibration methodology explained in Fig. 1e, constant A and B in the L(N$_f$) relationship, Eq. (2), were estimated for P$_S$ = 50% via the un-notched plain fatigue curves and the fatigue curves determined by testing the specimens containing V-notches with root radius, ρ, equal

to 0.4 mm. This approach was followed to calibrate the L(N$_f$) relationship under both R = -1 and R = 0.1, obtaining:

$$L\left(N_f\right) = 1.252 \bullet N_f^{-0.057} \, [\mathrm{mm}] \text{ under } \mathrm{R} = -1 \tag{20}$$

$$L\left(N_f\right) = 0.171 \bullet N_f^{0.097} \, [\mathrm{mm}] \text{ under } \mathrm{R} = 0.1 \tag{21}$$

Table 1
Summary of the fatigue curves determined by post-processing the experimental data generated by testing plain and notched specimens of AM Ti6Al4V (K_t is the stress concentration factor referred to the net area).

ρ [mm]	w_g [mm]	w_n [mm]	t [mm]	K_t	R	k	$\Delta\sigma_0$ or $\Delta\sigma_{0n}$ [MPa]	$T\sigma$
–	12.1	4.6	2.7	1.00	−1	2.8	105.6	1.94
					0.1	3.3	114.1	1.98
1.5	12.1	6.0	2.7	2.10	−1	2.8	88.8	3.27
					0.1	3.7	104.2	3.54
0.7	12.1	5.8	2.7	2.86	−1	1.5	36.7	7.32
					0.1	4.8	107.1	2.21
0.4	12.1	4.7	2.7	3.37	−1	2.6	69.6	1.70
					0.1	3.9	84.6	1.83

Relationships (20) and (21) are plotted also in the chart of Fig. 6. According to this chart, the critical distance displays limited variation as the number of cycles to failure increases, with this holding true under both R = -1 and R = 0.1. This suggests that the critical distance can be assumed to be constant in the fatigue lifetime interval of interest, with this resulting just in a little loss of accuracy. This simplifying assumption was then used to post-process relationships (20) and (21), obtaining for both the R = -1 and the R = 0.1 case an average value, L_{av}, for the critical distance of about 0.6 mm. Thus, the hypothesis was formed that, for the specific AM titanium alloy being tested, constant B in Eq. (2) could be taken invariably equal to zero so that:

$$L(N_f) = L_{av} = 0.6 \text{ mm under both } R = -1 \text{ and } R = 0.1 \qquad (22)$$

This average value for the critical distance was then employed to post-process the generated notch fatigue results according to the Point, the Line and the Area Method. The overall accuracy obtained by using these three different formalisations of the TCD is summarised in the experimental, N_f, vs estimated, $N_{f,e}$, fatigue lifetime diagrams seen in Fig. 7a to 7c. In particular, the error diagram of Fig. 7b shows that the TCD used in the form of the Line Method returned estimates all falling within the parent material scatter bands. The use of the TCD in the form of both the Point Method (Fig. 7a) and the Area Method (Fig. 7c) returned instead estimates that were still accurate, but all characterised by a slight degree of conservatism.

To assess the accuracy of GE in predicting the fatigue lifetime of the tested notched specimens, initially length scale ℓ was estimated for the AM Ti-alloy under investigation via Eqs. (11) and (22), obtaining:

$$\ell(N_f) \approx \frac{1}{2\sqrt{2}} L(N_f) = \frac{1}{2\sqrt{2}} L_{av} = 0.21 \text{ mm under both } R = -1 \text{ and } R = 0.1 \qquad (23)$$
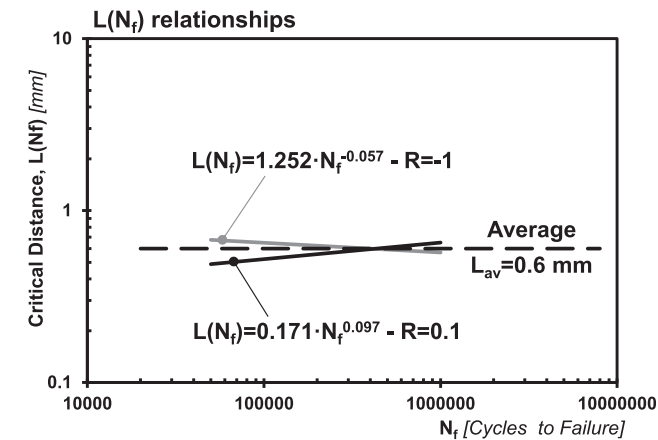

Fig. 6. L(N_f) relationships obtained according to the procedure summarised in Fig. 1e by post processing the plain fatigue results together with the results generated by testing the sharply notched specimens.

Subsequently, a number of numerical analyses with GE were carried out to determine the relevant gradient-enriched stress fields. To this end, the stress-based staggered approach of Eqns. (10a) and (10c) was adopted, where both steps lend themselves straightforwardly to implementation with standard finite element technology. Three-noded linear triangles were used within a plane stress framework. The gradient-enriched stresses at the tip of the notch were retrieved directly as nodal data from the numerical results of Eq. (10c) without any need for further post-processing. The ranges of the gradient-enriched stresses at the notch tip, $\Delta\sigma_{GE,y}$, were then directly used along with the parent material fatigue properties to estimate the fatigue lifetime of the notched specimens being tested, i.e.:

$$N_{f,e} = N_0 \left(\frac{\Delta\sigma_0}{\Delta\sigma_{GE,y}} \right)^k \qquad (24)$$

The error chart seen in Fig. 7d makes it evident that the estimates obtained via GE as well were highly accurate, even if slightly conservative. This trend is not at all surprising, since the use of GE is seen to be characterised by a certain level of conservatism also when this elegant and powerful approach is used to estimate fatigue lifetime of conventional notched engineering materials [33,34].

Numerical FE models similar to those employed to apply the TCD were used to estimate also the ASED critical radius, R_0. As explained in Section 4, the calculation of R_0 was based on Eqs. (12) and (13) calibrated through the endurance limits (at $N_0 = 2 \bullet 10^6$ cycles) determined under both R = −1 and R = 0.1 by testing the plain samples as well as the sharply notched specimens ($\rho = 0.4$ mm) – see Table 1. This straightforward procedure returned a value of the control volume radius equal to 0.52 mm and to 0.42 mm under R = 0.1 and R = −1, respectively. Owing to the fact that these two values were very close to each other, similar to what was done to use the TCD, the ASED criterion was applied by setting R_0 equal to the average value from the two, i.e. $R_0 = 0.47$ mm. By post-processing the linear-elastic FE models, the ASED values were then calculated for the reference notched specimens, while Eq. (14) was used to model in terms of SED the fatigue behaviour of the plain material (under both R = −1 and R = 0.1).

It should be noted that due to the linear-elastic nature of the ASED criterion, according to Eqs. (14), (16) and (17) the strain energy density range is proportional to the square of the applied nominal stress range. Therefore, fatigue results expressed in terms of nominal stress ranges, $\Delta\sigma_{net}$, can easily be turned into ASED-based data via the following expression:

$$\Delta\overline{W} = \Delta\overline{W}|_{unitload} \bullet (\Delta\sigma_{net})^2 \qquad (25)$$

where $\Delta\overline{W}|_{unitload}$ is the ASED range determined from a numerical model solved by setting the range of the applied nominal stress equal to unity. Taking full advantage of this simplified procedure, the calibration data (i.e., plain specimens and notched specimens with $\rho = 0.4$ mm) expressed in terms of $\Delta\overline{W}$ and N_f were then post-processed together using a simple linear regression, obtaining:

$$c_w \Delta\overline{W} = 406.1 \bullet N_f^{-0.609} \text{ for } R = 0.1 \qquad (26)$$

$$c_w \Delta\overline{W} = 919.9 \bullet N_f^{-0.724} \text{ for } R = -1 \qquad (27)$$

Finally, from the relevant FE models solved by setting the nominal stress range invariably equal to unity, Eq. (25) was used together with Eq. (26) and Eq. (27) to post-process the notch results seen in Fig. 5 and generated under R = 0.1 and to R = −1, respectively. The comparison between experimental, N_f, and estimated, $N_{f,e}$, number of cycles to failure is presented in Fig. 7e. As per this chart, almost all the estimates fall within the parent material scatter bands. This confirms that the ASED criterion as well is highly accurate in estimating the fatigue lifetime of the tested notched specimens.
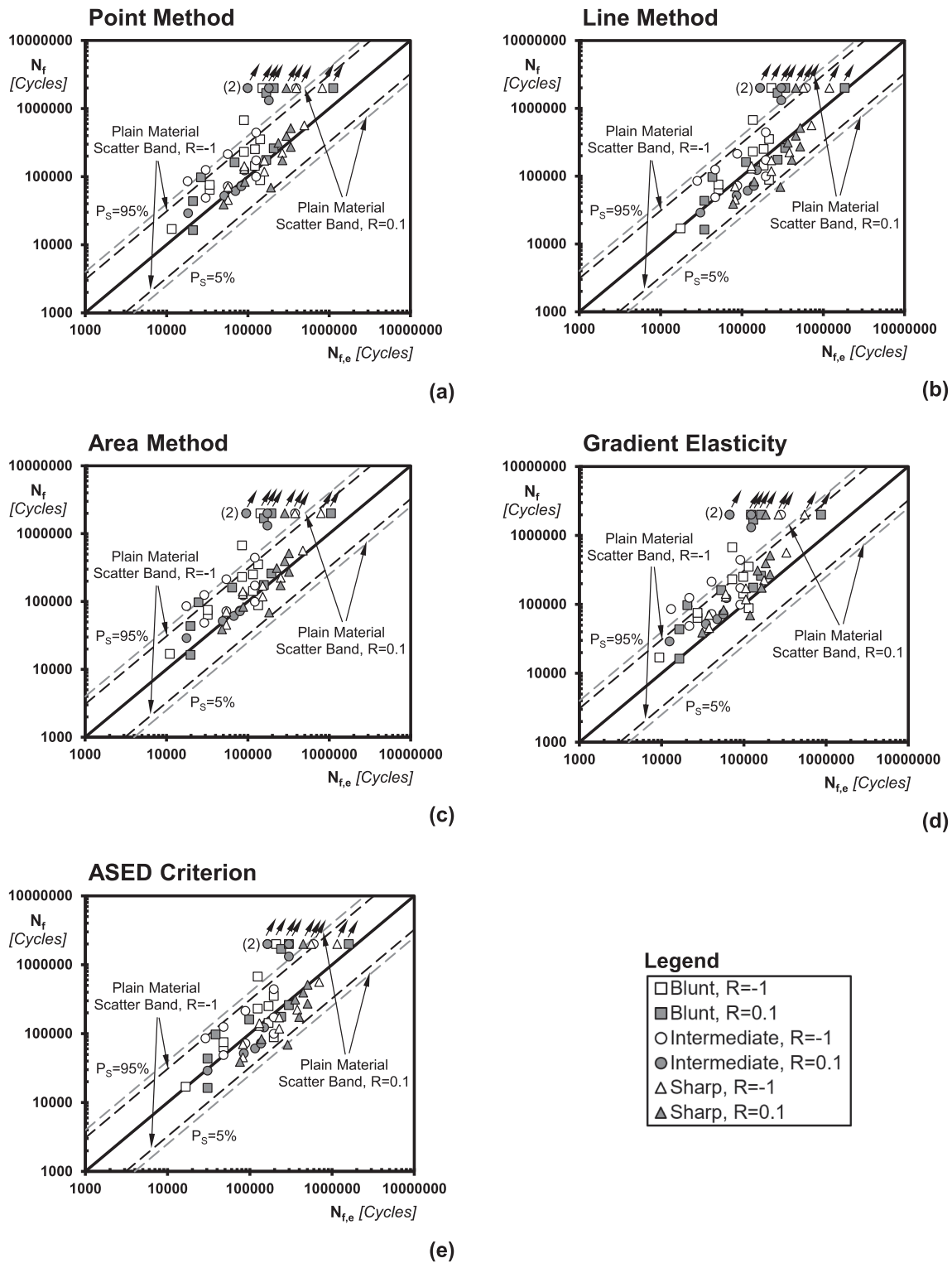
Fig. 7. Accuracy of the Point Method (a), Line Method (b), Area Method (c), Gradient Elasticity (d) and Averaged SED approach (e) in estimating the fatigue lifetime of the tested notched specimens of AM Ti6Al4V.

7. Conclusions

The present investigation aims at assessing the accuracy of three different length scale-based methodologies in predicting finite lifetime of notched AM Ti6Al4V. The notched specimens used to perform the validation exercise discussed in Section 6 were tested under load ratios equal to −1 as well as to 0.1. The accuracy and reliability of the TCD, GE and the ASED criterion in estimating fatigue lifetime of notched AM Ti6Al4V were checked systematically against the generated fatigue results.

Based on the outcomes from this experimental/theoretical work, the most relevant conclusions are summarised in what follows.

- Due to internal defects and superficial residual stresses, the inverse slope of the plain fatigue curves is close to the k values characterising the notch fatigue curves.
- The fatigue behaviour of the tested AM titanium alloy is affected by notch sharpness and magnitude of superimposed static stresses.
- Both in the presence and in the absence of notches, fatigue cracks are seen to initiate either on the surface or from sub-surface manufacturing defects.
- The TCD, GE and the ASED criterion are successful in estimating the fatigue lifetime of the tested notched specimens, with the estimates mainly falling within the plain material scatter bands.
- Length scale-based design methods allow fatigue assessment of notched AM to be performed by directly post-processing the relevant stress fields determined via conventional linear-elastic FE analyses.
- More work needs to be done to assess the accuracy of length scale-based design methods in estimating fatigue lifetime under variable amplitude fatigue loading.

Declaration of Competing Interest

The authors declare that they have no known competing financial interests or personal relationships that could have appeared to influence the work reported in this paper.

Data availability

Data directly avaialable in the paper

References

[1] Razavi SMJ, du Plessis A, Berto F. Structural integrity III: energy-based fatigue prediction for complex parts. In: Yadroitsev I, Yadroitsava I, Du Plessis A, MacDonald E, editors. Fundamentals of Laser Powder Bed Fusion of Metals. 1st Edition,. Oxford: Elsevier; 2021. p. 395–422.

[2] Kasperovich G, Hausmann J. Improvement of fatigue resistance and ductility of TiAl6V4 processed by selective laser melting. J Mater Process Technol 2015;220: 202–14.

[3] Li P, Warner DH, Fatemi A, Phan N. Critical assessment of the fatigue performance of additively manufactured Ti-6Al-4V and perspective for future research. Int J Fatigue 2016;85:130–43.

[4] Leuders S, Thöne M, Riemer A, Niendorf T, Tröster T, Richard HA, et al. On the mechanical behaviour of titanium alloy TiAl6V4 manufactured by selective laser melting: fatigue resistance and crack growth performance. Int J Fatigue 2013;48: 300–7.

[5] Haider A, Ma L, Ghadbeigi H, Mumtaz K. In-situ residual stress reduction, martensitic decomposition and mechanical properties enhancement through high temperature powder bed pre-heating of Selective Laser Melted Ti6Al4V. Mater Sci Eng A 2017;695:211–20.

[6] Razavi SMJ, Berto F. Directed energy deposition versus wrought Ti-6Al-4V: a comparison of microstructure, fatigue behavior, and notch sensitivity. Adv Eng Mater 2019;21(8):1900220.

[7] Vilaro T, Colin C, Bartout JD. As-fabricated and heat-treated microstructures of the Ti-6Al-4V alloy processed by selective laser melting. Metall Mater Trans A 2011;42 (10):3190–9.

[8] Masuo H, Tanaka Y, Morokoshi S, Yagura H, Uchida T, Yamamoto Y, et al. Influence of defects, surface roughness and HIP on the fatigue strength of Ti-6Al-4V manufactured by additive manufacturing. Int J Fatigue 2018;117:163–79.

[9] Maleki E, Bagherifard S, Bandini M, Guagliano M. Surface post-treatments for metal additive manufacturing: Progress, challenges, and opportunities. Addit Manuf 2021;37:101619.

[10] Berto F, Razavi SMJ, Torgersen J. Frontiers of fracture and fatigue: Some recent applications of the local strain energy density. Frat Integrita Strutt 2018;12(43): 1–32.

[11] Santecchia E, Hamouda AMS, Musharavati F, Zalnezhad E, Cabibbo M, El Mehtedi M, et al. A Review on Fatigue Life Prediction Methods for Metals. Adv Mater Sci Eng 2016;2016:1–26.

[12] Tanaka K. Engineering formulae for fatigue strength reduction due to crack-like notches. Int J Fracture 1983;22(2):R39–46.

[13] Taylor D. Geometrical effects in fatigue: a unifying theoretical model. Int J Fatigue 1999;21(5):413–20.

[14] Taylor D. The Theory of Critical Distances: A New Perspective in Fracture Mechanics. Elsevier Science; 2007.

[15] Susmel L. The Theory of Critical Distances: a review of its applications in fatigue. Eng Frac Mech 2008;75(7):1706–24.

[16] Susmel L. Multiaxial notch fatigue: from nominal to local stress–strain quantities. Cambridge (UK): Woodhead & CRC; 2009.

[17] Bellett D, Taylor D, Marco S, Mazzeo E, Guillois J, Pircher T. The fatigue behaviour of three-dimensional stress concentrations. Int J Fatigue 2005;27(3):207–21.

[18] Susmel L. A unifying approach to estimate the high-cycle fatigue strength of notched components subjected to both uniaxial and multiaxial cyclic loadings. Fatigue Fract Engng Mater Struct 2004;27(5):391–411.

[19] El Haddad MH, Topper TH, Smith KN. Fatigue crack propagation of short cracks. J Engng Mater Tech (ASME Trans) 1979;101:42–5.

[20] Susmel L, Taylor D. A novel formulation of the Theory of Critical Distances to estimate Lifetime of Notched Components in the Medium-Cycle Fatigue Regime. Fatigue Fract Eng Mater Struct 2007;30(7):567–81.

[21] Susmel L, Taylor D. The Theory of Critical Distances to estimate lifetime of notched components subjected to variable amplitude uniaxial fatigue loading. Int J Fatigue 2011;33(7):900–11.

[22] Sheppard SD. Field effects in fatigue crack initiation: long life fatigue strength. ASME J Mech Des 1991;113:188–94.

[23] Aifantis EC. On the role of gradients in the localization of deformation and fracture. Int J Engng Sci 1992;30(10):1279–99.

[24] Altan SB, Aifantis EC. On the structure of the mode III crack-tip in gradient elasticity. Scripta Metall Mater 1992;26(2):319–24.

[25] Ru CQ, Aifantis EC. A simple approach to solve boundary-value problems in gradient elasticity. Acta Mech 1993;101(1-4):59–68.

[26] Eringen AC, Edelen DGB. On nonlocal elasticity. Int J Engng Sci 1972;10(3): 233–48.

[27] Eringen AC. Linear theory of nonlocal elasticity and dispersion of plane waves. Int J Engng Sci 1972;10(5):425–35.

[28] Eringen AC. On differential equations of nonlocal elasticity and solutions of screw dislocation and surface waves. J Appl Phys 1983;54(9):4703–10.

[29] Askes H, Morata I, Aifantis EC. Finite element analysis with staggered gradient elasticity. Comput Struct 2008;86(11-12):1266–79.

[30] Askes H, Aifantis EC. Gradient elasticity in statics and dynamics: an overview of formulations, length scale identification procedures, finite element implementations and new results. Int J Solids Struct 2011;48(13):1962–90.

[31] Susmel L, Askes H, Bennett T, Taylor D. Theory of Critical Distances versus Gradient Mechanics in modelling the transition from the short to long crack regime at the fatigue limit. Fatigue Fract Engng Mater Struct 2013;36:861–9.

[32] Askes H, Susmel L. Understanding cracked materials: is Linear Elastic Fracture Mechanics obsolete? Fatigue Fract Engng Mater Struct 2015;38:154–60.

[33] Jadallah O, Bagni C, Askes H, Susmel L. Microstructural length scale parameters to model the high-cycle fatigue behaviour of notched plain concrete. Int J Fatigue 2016;82:708–20.

[34] Bagni C, Askes H, Susmel L. Gradient elasticity: a transformative stress analysis tool to design notched components against uniaxial/multiaxial high-cycle fatigue. Fatigue Fract Eng Mater Struct 2016;39(8):1012–29.

[35] Lazzarin P, Zambardi R. A finite-volume-energy based approach to predict the static and fatigue behavior of components with sharp V-shaped notches. Int J Fract 2001;112:275–98.

[36] Berto F, Lazzarin P. Recent developments in brittle and quasi-brittle failure assessment of engineering materials by means of local approaches. Mater Sci Eng R 2014;75:1–48.

[37] Berto F, Lazzarin P. A review of the volume-based strain energy density approach applied to V-notches and welded structures. Theor Appl Fract Mech 2009;52(3): 183–94.

[38] Williams ML. Stress Singularities Resulting From Various Boundary Conditions in Angular Corners of Plates in Extension. J Appl Mech 1952;19(4):526–8.

[39] Lazzarin P, Livieri P, Berto F, Zappalorto M. Local strain energy density and fatigue strength of welded joints under uniaxial and multiaxial loading. Eng Fract Mech 2008;75(7):1875–89.

[40] Lazzarin P, Sonsino C, Zambardi R. A notch stress intensity approach to assess the multiaxial fatigue strength of welded tube-to-flange joints subjected to combined loadings. Fatigue Fract Eng Mater Struct 2004;27:127–40.

[41] Lazzarin P, Lassen T, Livieri P. A notch stress intensity approach applied to fatigue life predictions of welded joints with different local toe geometry. Fatigue Fract Eng Mater Struct 2003;26(1):49–58.

[42] Lazzarin P, Berto F. Some expressions for the strain energy in a finite volume surrounding the root of blunt V-notches. Int J Fract 2005;135:161–85.

[43] Lazzarin P, Berto F, Zappalorto M. Rapid calculations of notch stress intensity factors based on averaged strain energy density from coarse meshes: Theoretical bases and applications. Int J Fatigue 2010;32:1559–67.

[44] Anon.. Standard Practice for Statistical Analysis of Linear or Linearized Stress-Life (S-N) and Strain-Life (ε-N) Fatigue Data. ASTM E739 2015.

[45] Al Zamzami I, Susmel L. On the accuracy of nominal, structural, and local stress based approaches in designing aluminium welded joints against fatigue. Int J Fatigue 2017;101:137–58.

[46] Susmel L. On the estimation of the material fatigue properties required to perform the multiaxial fatigue assessment. Fatigue Fract Engng Mater Struct 2013;36: 565–85.

[47] Lee Y-L, Pan J, Hathaway RB, Barkey ME. Fatigue Testing and Analysis: Theory and Practice. Elsevier Butterworth-Heinemann; 2005.